^{4}He clusters adsorbed on graphene

L. Vranješ Markić,[1] P. Stipanović,[1] I. Bešlić,[1,2] and R. E. Zillich[3,4]
[1]*Faculty of Science, University of Split, HR-21000 Split, Croatia*
[2]*Departament de Física i Enginyeria Nuclear, Universitat Politècnica de Catalunya, Campus Nord B4-B5, E-08034 Barcelona, Spain*
[3]*Institut für Theoretische Physik, Johannes Kepler Universität, A 4040 Linz, Austria*
[4]*Institute for Quantum Optics and Quantum Information (IQOQI), Austrian Academy of Sciences, 6020 Innsbruck, Austria*
(Received 31 March 2012; revised manuscript received 6 August 2013; published 11 September 2013)

We report the results of a study of ^4He_N clusters, for $2 \leqslant N \leqslant 40$, adsorbed on one and both sides of a graphene sheet. The ground-state properties are determined using variational and diffusion Monte Carlo calculations at zero temperature, and in addition path integral Monte Carlo simulations at finite temperature are performed for some selected cluster sizes. For the interaction of helium atoms with graphene, we compare several models: a smooth He-graphene potential that depends only on the distance to the graphene sheet and potentials constructed as a sum of individual He-C interactions where two possibilities for this He-C interaction are tested. In this way, we assess the effect of corrugation on the binding properties of helium clusters. Furthermore, we study the influence that the graphene-mediated McLachlan dispersion energy has on the He-He interaction. The McLachlan interaction weakens the attraction between helium atoms, which turns out to have a significant effect on the binding energy and the shape of adsorbed ^{4}He clusters. We find that clusters adsorbed on opposite sides of graphene are bound, but according to the He-He pair distribution function across the graphene sheet, pair correlations are very weak. For a large enough number of particles, solidlike $\sqrt{3} \times \sqrt{3}$ structures start to become energetically preferred for the model of anisotropic corrugation without the McLachlan interaction. For the other models, the ground state of the studied clusters is clearly liquidlike.

DOI: 10.1103/PhysRevB.88.125416 PACS number(s): 67.25.dr, 68.43.Fg, 67.25.bh, 36.40.−c

I. INTRODUCTION

In 2004, graphene, which is a single layer of a graphite plane, was isolated for the first time.[1] Since then, because of its surprising mechanical, structural, and electronic properties, it has become a major focus in material science. Graphene is a particularly interesting candidate for future electronic applications at the nanometer scale. Adsorption of gas molecules changes the electrical conductivity of graphene.[2] It was demonstrated that graphene can be used as a sensitive gas sensor, capable of detecting individual molecules.[2] Furthermore, the study of effects of a physically adsorbed helium film on the conductivity of graphene[3] suggests that transport properties may be a good probe of the structure of an adsorbed film. The change in the electrical conductivity has already been used to monitor phase transitions of adsorbed Ar and Kr atoms on the surface of a single-carbon nanotube, which has in addition been shown to behave as a nanoscale resonator capable of detecting adsorption at the level of single atoms.[4] Free-standing epitaxial graphene has already been synthesized,[5] which opens prospects for experimental investigations of systems adsorbed on both sides, including experiments similar to adsorption on a single nanotube.

Graphene also offers the possibility to study adsorbed quantum systems of reduced dimensionality, which is also interesting from a fundamental point of view. The prospect of observing a single layer of superfluid liquid helium attracted a lot of effort to the study of helium on graphite, both experimentally and theoretically. Finally, the first layer was found to be a $\sqrt{3} \times \sqrt{3}$ commensurate solid.[6] Some ambiguity remained regarding the phase of helium at submonolayer densities. In a path integral Monte Carlo (PIMC) study, Pierce and Manousakis[7] found that a low-density submonolayer of ^{4}He on graphite consists of solid clusters and a low-density vapor. The paper questioned an interpretation of experimental results by Greywall and Bush[8] in favor of the superfluid phase and offered the alternative explanation involving solid clusters.

Recently, Gordillo and Boronat[9] studied adsorbed ^{4}He on one side of graphene by quantum Monte Carlo (QMC) simulations at zero temperature. The energy difference between a $\sqrt{3} \times \sqrt{3}$ commensurate solid and a liquid phase was found to be very small. Considering the uncertainties of three-body effects on the He-He interactions, the possibility was left open that a liquid ^{4}He monolayer could be stable. In addition, Gordillo and Boronat studied the superfluid density of the first layer of ^{4}He and H_2 adsorbed on both graphene and graphite.[10] In contrast to the case of H_2, in a perfect solid phase a small superfluid fraction was observed (0.67%) for ^{4}He, which increased with the introduction of vacancies while not destroying the spatial solid order.

The model used to describe the interactions between adsorbate and substrate atoms as well as between adsorbed atoms can have an effect on the predictions of the stable phase. On graphite it was found that it is necessary to include corrugation, i.e., the modulation of the graphene-He interaction parallel to the substrate surface, in the calculation in order to obtain the low-density ^{4}He solid phase.[7,11] The simulation of helium monolayers adsorbed on a laterally averaged, i.e., smooth, graphite potential,[12] similar to the studies of helium in two dimensions (2D),[13,14] found that the equilibrium phase was liquid, at a density of around 0.04 Å^{-2}.

In the study of ^{4}He adsorption on graphene, Gordillo and Boronat used the corrugated potential constructed as a sum of isotropic pair potentials, but did not include the graphene-mediated (McLachlan) dispersion interaction, which at the time was only available for graphite. Recently, Bruch *et al.*[15] determined leading perturbation terms of the McLachlan

energy of two atoms in the presence of a graphene sheet. The inclusion of this interaction, which reduces the He-He attraction, is expected to decrease the stability of the commensurate solid relative to a spatially modulated low-density monolayer liquid. However, on graphite, Pierce and Manousakis[16] did not find a qualitative change in their predictions for the first helium layer, in contrast to the variational calculation of Gottlieb and Bruch[11] which showed that even in the corrugated case, liquid became the preferred phase. Gordillo and Boronat[9] included the graphite McLachlan interaction in the study of the first layer of ^{4}He adsorbed on eight layers of graphene. They found that solid remained the preferred phase but with an even smaller difference than without the substrate-mediated interaction.

In the case of graphite, if the interaction with He is modeled by *anisotropic* pair potentials, the corrugation amplitude increases significantly.[17] Such a large corrugation amplitude is supported by results coming from selective adsorption helium scattering experiments and by the low-density monolayer specific-heat experiments in the case of graphite.[18] The anisotropy in He-C interaction for graphene was explored recently by Kwon and Ceperley.[19] They found that the monolayer of helium forms a commensurate solid with both isotropic and anisotropic potential, however, when vacancies are introduced the phases are qualitatively different. Results with the anisotropic potential are consistent with the existence of commensurate solid clusters, while in the case of the isotropic potential the existence of delocalized vacancies and a finite value of the superfluid fraction support the interpretation of a liquid phase. Such differences in the predictions of helium properties using isotropic and anisotropic He-C potential were not found in the study of the second layer of helium on graphene by Gordillo and Boronat.[20] This is not surprising because the second layer being further from the graphene sheet is much less influenced by the corrugation effects. The latest results of Gordillo and Boronat confirm that with the anisotropic potential, the first-layer solid is stabilized with respect to a liquid phase.[21]

Apart from pure carbon substrates, adsorption of helium and para-hydrogen has also been studied for graphane (where a H atom is bonded to each C) and fluorographene substrates where novel phases such as an anisotropic superfluid ^{4}He film have been predicted for these honeycomb lattice substrates[22–24] (see also the review Ref. 25).

The prospect of adsorption experiments on graphene, which would be capable of achieving single-atom resolution, suggests the need for determining the binding properties of a small number of helium atoms on the surface of graphene. In several works, liquid-helium clusters adsorbed on flat surfaces were studied using two-dimensional models[26–28] which did not include corrugation. These studies also showed that extrapolated central cluster densities and energies per particles gave a good agreement with bulk liquid calculations. Very small clusters on graphite with up to four atoms were also studied for the laterally averaged helium-graphite potential,[29,30] where it was found that their properties are very close to those obtained in 2D calculations.[29] Finite helium clusters were recently studied adsorbed on C_{20} and C_{60} fullerenes using PIMC simulations where the isotropic He-C interaction potential for graphite was employed.[31,32] Depending on the number of atoms adsorbed on C_{20}, clusters with both fluid and solid order were observed. The first layer of ^{4}He exhibited a commensurate solid structure for $N = 32$ adsorbed atoms, and a finite superfluid fraction was observed if vacancies were present. Similarly, for ^{4}He on C_{60} a commensurate solid order was also obtained for $N = 32$. The increase in the number of atoms leads to a commensurate-incommensurate transition, after passing through various domain-wall structures, demonstrating that the physical properties on the larger fullerene surface approach those of the flat layer of helium adsorbed on graphite.

In this work, we present a study of the ground state of weakly bound small $^4\mathrm{He}_N$ clusters, for N up to 40, adsorbed on one and both sides of graphene. We conducted an extensive survey of the influence of the graphene-He interaction model and the graphene-mediated McLachlan interaction on the energetics and the structure of the clusters. We determine the effects of adsorption on both sides of graphene on the properties of clusters, and quantify the correlations between two clusters adsorbed on opposite sides. We also address the question as to whether the ground state of the clusters is solid or liquid. The calculations are performed at zero temperature using variational and diffusion Monte Carlo (VMC and DMC, respectively) simulations. For selected cluster sizes, calculations are also performed at finite temperatures using PIMC simulations.

We introduce the methods and the interaction potential models in Sec. II. In Sec. III, we discuss the adsorption of a single ^{4}He atom. Results concerning the ground-state energy of ^{4}He liquidlike clusters adsorbed on one side are reported in Sec. IV, and on both sides in Sec. V. We discuss the stability of liquid versus solid clusters in Sec. VI.

II. METHOD

^{4}He clusters adsorbed on one and both sides of graphene are described by an N-particle Hamiltonian

$$H = -\frac{\hbar^2}{2m}\sum_{i=1}^{N}\nabla_i^2 + \sum_{i<j}^{N} V(r_{ij}) + \sum_{i=1}^{N} V_s(\boldsymbol{r_i}), \qquad (1)$$

where $V(r_{ij})$ is the interaction potential between helium atoms and $V_s(\boldsymbol{r_i})$ is the interaction potential between He atoms and graphene. For bulk helium, He-He interactions are very well described by the Aziz HFD-B(He) potential.[33] However, for helium adsorbed on a substrate, the direct He-He interaction is modified by substrate-mediated interactions. Previous studies of He adsorbed on graphite[11,16] showed that it is important to consider the substrate-mediated McLachlan dispersion energy,[34] which arises from the screened electrodynamic response of the substrate to the fluctuating electric dipoles of the adsorbed atoms. We also include this effect, using a model recently proposed by Bruch *et al.*[15] Since the expression for the interaction, i.e., Eq. (14) in the paper of Bruch *et al.*, contains one typographical error, we give here the full corrected expression. For two adatoms with coordinates (x_a, y_a, z_a) and (x_b, y_b, z_b), the McLachlan interaction is given

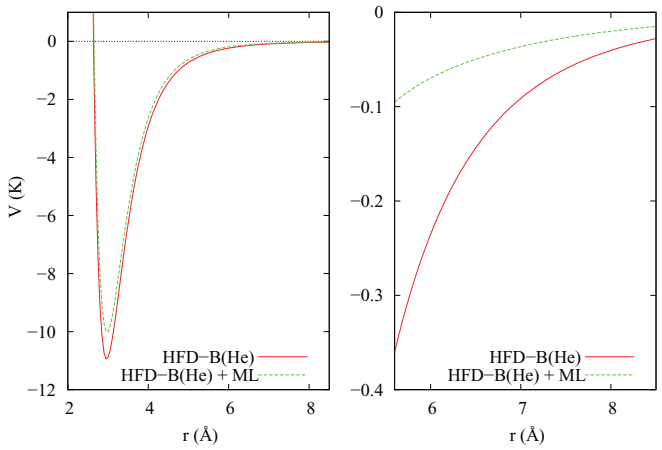

FIG. 1. (Color online) The interaction potential between two He atoms as function of their (three-dimensional) separation. On the left, both atoms are on the same side of graphene, and on the right they are on opposite sides. The solid curves show the HFD-B(He) interaction by Aziz *et al.* (Ref. 33) and the dashed curves include the graphene-mediated additional McLachlan interaction (Refs. 15 and 34). The He atoms are at a distance of 2.8 Å from the graphene surface.

by the expressions

$$V_{\rm ML} = 2C_{p1+}\frac{z_+}{r^3R_I^5}\left[6-5\frac{z_+^2}{R_I^2}-3\frac{(z_a-z_b)^2}{r^2}\right] - 12\frac{C_{p2+}}{R_I^8}\left[1+2\frac{z_+^2}{R_I^2}\right], \quad z_a \geqslant z_b > z_c$$
$$= -6\frac{C_{p1-}}{r^8}(z_a-z_b) - 3\frac{C_{p2-}}{r^{10}}[r^2+2(z_a-z_b)^2], \quad z_a > z_c > z_b$$

where r is the distance between the adatoms, z_c is the location of the graphene plane, which we take to be at $z_c = 0$, $z_+ \equiv z_a + z_b - 2z_c$, $R_I^2 = [(x_a-x_b)^2 + (y_a-y_b)^2 + z_+^2]$, and $C_{p1+}, C_{p2+}, C_{p1-}, C_{p2-}$ are dipole strengths with values taken from Ref. 15. In the derivation, several approximations are introduced, which means that the McLachlan interaction is not as accurate as the HFD-B(He) potential. In the following, we abbreviate the McLachlan interaction as ML. Figure 1 shows the He-He interaction potential for two He atoms, both 2.8 Å away from the surface, which is approximately the maximum of the single-particle wave function. On the left, both atoms are on the same side of the graphene sheet, and on the right they are on opposite sides. The potential between two He atoms on the same side is reduced by about 1 K in the potential well when the ML interaction is included, corresponding approximately to a 10% reduction. Hence, the bare He-He interaction is much larger than the ML correction. While such a small modification of the effective pair interaction would not lead to a qualitative change of the properties of most condensed systems, for ^{4}He a 10% reduction is expected to have important implications. Due to the large cancellation of potential and kinetic energy, the change of the total binding energy can be much larger than 10%. Furthermore, in three dimensions the He-He interaction has a resonance near zero energy which means that the (single) bound state of a pair of ^{4}He atoms has a very small binding energy, i.e., that two ^{4}He atoms are barely bound. Also, in two dimensions, a pair of He atoms is very weakly bound, thus the ML interaction should have a major impact on the properties of small clusters. For two He atoms on opposite sides, the right panel of Fig. 1 shows that the relative reduction of the attraction is substantial when the ML interaction is taken into account, with the effective He-He interactions weakened by about a factor of 4 relative to the bare He-He interaction. Let us note that another form of substrate-mediated interaction exists, the Kohn-Lau energy,[35] which arises from the elastic distortion of the substrate by the adsorbate. The study of helium adsorption on graphite showed it had a much smaller effect than the ML interaction.[11] Recently, it has been suggested that it may be much more important for graphene due to the flexibility of the substrate.[25] However, since a model for this interaction for graphene is not available, we have not been able to study its effects.

For the interaction between He atom and the graphene substrate, we use three different models. First, we consider a laterally averaged graphene-He interaction, giving rise to a smooth substrate model. Second, we consider corrugation by forming the graphene-He potential as a sum of individual He-C interactions. This second model (labeled Iso) is referred to as isotropic corrugation, arising as a sum of Lennard-Jones He-C interactions with parameters taken from Stan and Cole.[36] A better description of the corrugated graphene surface is obtained by generalizing the individual He-C interactions to anisotropic interactions, using the 6-12 anisotropic potential of Carlos and Cole with anisotropy parameters $\gamma_A = 0.4$ and $\gamma_R = -0.54$ (see Ref. 17 for details); this third model is labeled AnIso. The minimum of the graphene-He potential is -192 K in the case of the Iso model and -205 K in the case of the AnIso model.

Combining these three graphene-He interaction models with the choice of omitting (/0) or including (/ML) the substrate-mediated ML interaction, we obtain six different models for describing ^{4}He clusters adsorbed on graphene. Using the abbreviations introduced above, we have the smooth/0, smooth/ML, Iso/0, Iso/ML, AnIso/0, and AnIso/ML models.

For the study of clusters at zero temperature, we use VMC calculations followed by DMC calculations. The starting point of the DMC method is the Schrödinger equation written in imaginary time,

$$-\hbar\frac{\partial\Psi(\boldsymbol{R},t)}{\partial t} = (H - E_{\rm r})\Psi(\boldsymbol{R},t), \qquad (2)$$

which is solved stochastically. In Eq. (2), t is the imaginary time and $E_{\rm r}$ is a reference energy, while $\boldsymbol{R} \equiv (\boldsymbol{r}_1, \boldsymbol{r}_2, \ldots, \boldsymbol{r}_N)$ collectively denotes all particle positions. In order to reduce the variance to a manageable level, it is a common practice to use importance sampling by introducing a trial wave function $\psi(\mathbf{R})$. Then, the Schrödinger equation (2) is rewritten for the wave function $\Phi(\boldsymbol{R},t) = \Psi(\boldsymbol{R},t)\psi(\boldsymbol{R})$. Within the Monte Carlo framework, $\Phi(\boldsymbol{R},t)$ is represented by a set of *walkers*. In the limit $t \to \infty$ (for long simulation times), only the lowest-energy eigenfunction that is not orthogonal to $\psi(\mathbf{R})$ survives. This allows the calculation of ground-state expectation values by stochastic sampling. Apart from statistical uncertainties, the exact ground-state energy of an N-body bosonic system can thus be obtained.

In order to study liquidlike clusters, we use wave functions of Jastrow form, constructed as a product of two-body correlation functions $F(r)$, multiplied by single-particle functions describing binding of ^{4}He atoms on the substrate $\phi(\boldsymbol{r_i})$:

$$\psi(\boldsymbol{R}) = \prod_{i<j=1}^{N} F(r_{ij}) \prod_{i=1}^{N} \phi(\boldsymbol{r_i}). \tag{3}$$

For the atoms on the same side of the graphene sheet, two-body correlations are described by the ansatz

$$F(r) = \exp\left[-\frac{1}{2}\left(\frac{b}{r}\right)^5 - \frac{sr}{2}\right], \tag{4}$$

where r is the interparticle distance, and b and s are variational parameters. Atoms on opposite sides of graphene are too far apart to experience the repulsive part of the interaction, therefore it is sufficient to take into account only the exponentially decaying part of the correlations

$$F(r) = \exp\left(-s_1 r/2\right), \tag{5}$$

where s_1 is a variational parameter.

With DMC it is possible to study not just liquidlike, but also solidlike clusters by choosing an appropriate trial wave function. We model solidlike clusters using the Nosanow-Jastrow wave function

$$\psi_{\mathrm{NJ}}(\boldsymbol{R}) = \psi(\boldsymbol{R}) \prod_{i}^{N} h(\rho_{iI}), \tag{6}$$

where $h(\rho) = \exp(-\alpha\rho^2/2)$ laterally localizes every atom i to a fixed lattice point $\boldsymbol{\rho}_I$. The parameter α is optimized variationally, as well as the locations of the lattice points.

In order to obtain the ground state of a single adsorbed atom, the one-body Schrödinger equation has to be solved. In the case of the smooth graphene potential, the equation is one dimensional, and the wave function which depends only on the distance to the substrate $\phi(z)$ is obtained. For the one-body problem with corrugation, the ground state is obtained by imaginary-time propagation of the discretized three-dimensional wave function. The comparison between the wave functions in the Iso and the AnIso models is shown in Fig. 2. The periodicity of the substrate is visible. The difference between maxima and minima is larger in the case of anisotropic corrugation, but the wave function does not go to zero in either case. The effective mass of a single adsorbed ^{4}He atom is increased only by about 3% or 6% for the Iso or AnIso models, respectively.

The Jastrow wave function $\psi(\boldsymbol{R})$ [Eq. (3)] is optimized using the VMC method in the case of the smooth potential. The same parameters are then used in calculations with the corrugated potentials. In VMC, typically 70%–85% of the DMC energy is obtained for calculations without the ML interaction and around 5% less in calculations with the ML interaction. The difference between VMC and DMC results increases with the number of atoms in the cluster, except for the dimer ^{4}He$_2$ with up to two ^{4}He atoms adsorbed on the other side of the graphene sheet, and the ML interaction included. In that case, due to the very small binding energy and the large spatial extent of the wave function, our best VMC energies are only around 40%–60% of the DMC energy.

Without the ML interaction, we obtained the optimal value of parameter b around 3.05 Å and of parameter s in the range from 0.2 Å^{-1} for $N = 2$ to 0.009 Å^{-1} for $N = 40$. The optimal value of parameter s_1 ranges from 0.06 to 0.0015 Å^{-1}, and there are small changes of variational parameters b and s when the cluster is adsorbed on the other side of the graphene sheet. With the ML interaction included, the total He-He interaction potential becomes weaker which affects mostly parameters s and s_1. The optimal value of parameter s then ranges from 0.11 Å^{-1} for $N = 2$ to 0.0064 Å^{-1} for $N = 40$, while the optimal value of parameter s_1 ranges from 0.018 Å^{-1} for $N = 1$ to 0.0012 Å^{-1} for the largest clusters considered. In the case of the AnIso model, simulations were performed for solidlike clusters using the trial wave function (6). We found the optimal value of the parameters are $b = 2.8$ Å , $s = 0.016$ Å^{-1}, $s_1 = 0.001$ Å^{-1}, and $\alpha = 0.7$ Å^{-2} at the VMC level. DMC simulations were performed for several values of α to assure that the final conclusion is not biased by the choice of the parameters. For the AnIso/0 model and 37 particles it was found that slightly lower energies (around 2%) are obtained with α from 0.3 to 0.5 Å^{-2}. This can be explained by the fact that atoms on the edge are more delocalized than atoms in the inner part of the cluster, as observed by our PIMC simulations, and thus not so well described by the trial wave function with $\alpha = 0.7$ Å^{-2}. Using a reasonable number of walkers, for $\alpha = 0.7$ Å^{-2} DMC is not able to completely correct the parts of the trial wave function which are close to zero, hence in the case of the small solidlike clusters we find it is actually more

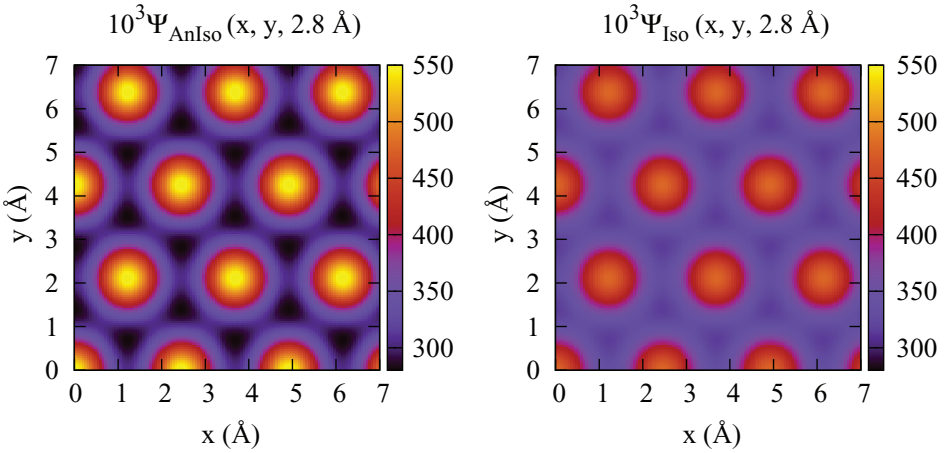

FIG. 2. (Color online) The wave functions for the ground state of a single ^{4}He atom adsorbed on graphene. The left panel is for the anisotropic corrugation (AnIso model) and the right panel for the isotropic corrugation (Iso model).

efficient to use a parameter which does not give the optimal VMC energy. For 20 particles in the AnIso/0 model, as well as for all N in the other models, the DMC energy decreased as α was reduced, towards the energy values obtained using the liquidlike trial wave function (corresponding to $\alpha = 0$).

We use a DMC method which is accurate to second order in the time step Δt.[37] Both the time-step dependence and the mean walker population are studied carefully in order to eliminate any bias. We adjust the mean number of walkers to the size of the ^{4}He cluster. For most of the clusters, 2000 walkers have proven to be enough, but for clusters with 40 atoms and the ML interaction included we increase the number to 12 000. The necessary increase of the mean number of walkers correlates with a reduced quality of the importance sampling wave function, reflected in the quality of the VMC results. In calculations with the corrugated models, typically 1000–3000 more walkers are used than in calculations with the smooth model. The energies are calculated for different time steps (from 2×10^{-4} K^{-1} to 14×10^{-4} K^{-1}) and the final results are derived by extrapolation to zero time step. For larger clusters, the upper range of the time-step values is reduced.

The density profiles and the pair distribution functions of the clusters are calculated using pure estimators,[38] where we verify that the chosen block size is large enough to correct the bias coming from the choice of the trial wave functions. Typically, 10 000 steps per block are used.

For PIMC simulations, we use the methodology of Ref. 39. For the He-He interaction, the short-time (high-temperature) N-body density matrix is approximated by the pair density scheme. For the graphene-He interaction, we use the simpler Trotter approximation. PIMC simulations for weakly bound clusters, as the ones studied here, are computationally expensive because very low temperatures are required to prevent evaporation. Furthermore, PIMC does not use a trial wave function that guides (but may also bias) the random walk. The PIMC method therefore faces similar challenges here as for simulations of ^{4}He clusters doped with weakly bound atoms or molecules which were performed for Rb and Rb_2 attached to ^{4}He clusters and films.[40–42] Therefore, we employ similar strategies for the present problem. The PIMC simulations are performed for very low temperature, namely, $T = 0.078$ K for $N = 20$. As the binding energy per particle increases with N (see below), evaporation is effectively prevented already at higher temperatures for larger cluster sizes. Therefore, we set $T = 0.156$ K in simulations for $N = 37$. We use time steps of $\Delta\tau = 1/40$ K (corresponding to paths with 512 beads), $1/80$ K (1024 beads), and for the most delicate case of $N = 20$ using the AnIso/0 model $1/160$ K (2048 beads). This allows for an approximate extrapolation to zero time step. Permutation sampling is used in all simulations to account for the Bose symmetry of ^{4}He atoms.

III. ADSORPTION OF A SINGLE ^{4}He ATOM

QMC simulations of a cluster of N ^{4}He atoms adsorbed on graphene yields the total ground-state energy E_N^T of the cluster which includes the graphene-He potential energy. Hence, the total cluster energy contains a contribution of N times the adsorption energy E_1^T of a single ^{4}He atom. This contribution is the vastly dominant part of E_N^T and is a simple single-particle property that is of little interest in our study of cluster properties. We therefore subtract it from E_N^T to reveal the more interesting many-body contributions to E_N^T. We define the *cluster energy*

$$E_N = E_N^T - N E_1^T. \tag{7}$$

Thus, E_N is the formation energy due to clustering of N ^{4}He atoms that are already adsorbed. If $E_N < 0$, there is a bound ground state of the cluster, while for $E_N = 0$ the cluster is not self-bound and ^{4}He atoms form a gaseous adsorbate.

TABLE I. Energy of a single ^{4}He atom adsorbed on graphene, E_1^T (in K), obtained for the three He-C interaction models (smooth, Iso, and AnIso).

	Smooth	Iso	AnIso
E_1^T	−127.318	−128.371	−129.864

The single-particle energy E_1^T and the associated wave function $\Psi_1(\mathbf{r})$ of a single ^{4}He atom adsorbed on graphene are calculated with the three graphene-He interaction models (smooth, Iso, AnIso). For corrugated models, the energy E_1^T and the wave function are obtained by solving the one-body Schrödinger equation by imaginary-time propagation towards the ground state. We use a discretization of $128 \times 256 \times 256$ grid points for a rectangular graphene cell containing 4 C atoms, of side length $\sqrt{3}a \times 3a$, where a is the C-C bond length of 1.42 Å. In the perpendicular direction, the lower and upper boundaries are 1.5 and 6.0 Å from the graphene plane, respectively. That is much larger than the perpendicular extent of the single-particle wave function $\Psi_1(\mathbf{r})$, which is stored together with its first and second derivatives and used in the trial wave function (3). E_1^T is tabulated in Table I. The value obtained in the Iso model agrees with the one given by Gordillo and Boronat,[9] who got -128.26 ± 0.04 K.

IV. ^{4}He LIQUIDLIKE CLUSTERS ON ONE SIDE

We first study ^{4}He clusters with up to $N = 40$ atoms adsorbed on just one side of graphene, using the trial wave function appropriate for a liquidlike cluster which is defined in Eq. (3). We stress that these clusters are effectively two dimensional, which is a consequence of the strong graphene binding. This means that, as we grow the cluster, the added particles spread only in the lateral direction. This can be contrasted with the case of helium clusters adsorbed on the much more weakly binding cesium surface[43] where the width of the cluster in the direction perpendicular to the substrate is several times larger [e.g., $\Delta z = \sqrt{\langle z^2\rangle - \langle z\rangle^2} = 0.3$ Å in case of $^4He_{20}$ cluster (AnIso/0) adsorbed on graphene and $\Delta z = 1.7$ Å for the same cluster on cesium using the Chimeshya, Cole and Zaremba (CCZ) potential as in Ref. 43].

Figure 3 presents the N dependence of the ground-state cluster energy per particle E_N/N obtained using the DMC method for the three graphene-He potentials (smooth, Iso, AnIso), with the ML interaction between ^{4}He atoms (right panel) and without it (left panel). The comparison of the results, obtained with the six different interaction models, shows that the omission or inclusion of the ML interaction

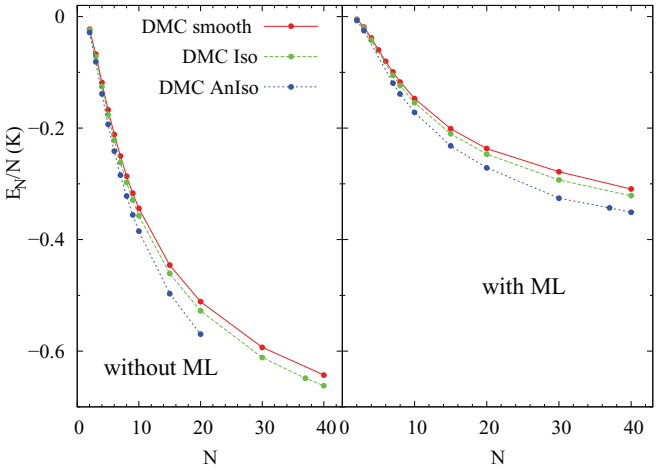

FIG. 3. (Color online) The ground-state energy per particle E_N/N of the clusters as a function of N. The presented DMC results are obtained using the six different interaction models (smooth/0, smooth/ML, Iso/0, Iso/ML, AnIso/0, and AnIso/ML).

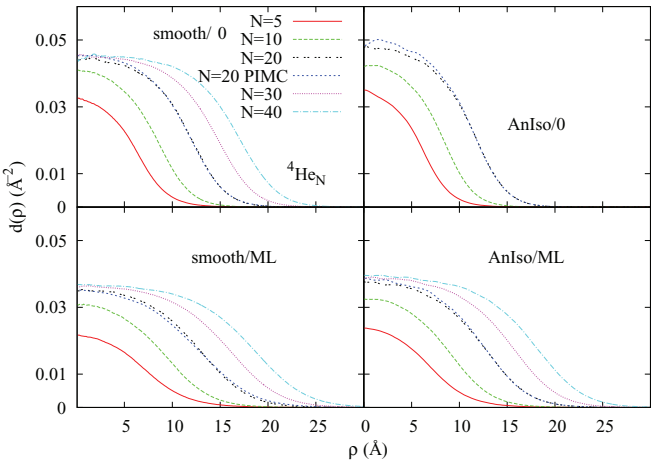

FIG. 4. (Color online) Density profiles $d(\rho)$ of ^{4}He clusters adsorbed on graphene. The results are obtained by the DMC simulations and in addition, for $N = 20$, by PIMC. The left and right panels correspond to the smooth and AnIso models. Top and bottom panels correspond to the cases of omitting and including the graphene-mediated ML interaction between ^{4}He atoms.

has a much stronger influence on the cluster energy than the model for the corrugation. If the ML interaction is included, E_N/N is only about half of the value obtained without the ML interaction. The choice of the graphene-He potential has much less influence on E_N/N, with the smooth and the Iso models giving almost the same energy, and the AnIso model resulting in slightly stronger binding. We note that the cluster energies E_N are about two orders of magnitude smaller than the total energy E_N^T, which includes the adsorption energy.

The ground-state energy E_N for the smooth/0 model can be compared either to the results for clusters in 2D,[26,27,29,44] or to the results for clusters adsorbed on a smooth graphite model.[30] We find slightly stronger binding than in 2D and almost the same as on graphite. For example, for $N = 4$, we have in 2D (Ref. 29) $E_4 = -435(1)$ mK, on graphite[30] $E_4 = -477(5)$ mK, and on graphene $E_4 = -473(4)$ mK (this work). The energies in 2D and on graphite were obtained using the more attractive He-He interaction potential by Korona *et al.*,[45] which means that on graphene the self-binding energies are slightly stronger than on graphite. This is to be expected since with respect to graphene the adsorption potential of graphite is stronger resulting in a slightly smaller width of the cluster perpendicular to the surface. It was shown for helium dimers in the model of harmonic holding potential that the self-binding is enhanced with respect to 2D, becoming stronger as the width of the confining potential is increased.[46] The study of ^{4}He$_{2,3,4}$ adsorbed on graphite and cesium[30] confirmed the harmonic model prediction.

In order to investigate structural properties of the clusters, we calculated the density profile $d(\rho)$ defined as the probability distribution of ^{4}He atoms with respect to a lateral distance ρ from the center of mass of the cluster

$$d(\boldsymbol{\rho}) = \sum_i \delta[\boldsymbol{\rho} - (\boldsymbol{\rho}^i - \boldsymbol{\rho}^{\text{c.m.}})].$$

For the smooth model, $d(\boldsymbol{\rho})$ does not depend on the direction of $\boldsymbol{\rho}$. For the two corrugated models, there will be a dependence on $\boldsymbol{\rho}$ due to the breaking of cylindrical symmetry on a substrate with C_6 symmetry. Since the corrugation for a light particle like ^{4}He is effectively small (the effective mass increases around 3% and 6% for a single ^{4}He on graphene using the Iso and AnIso models, respectively), the direction dependence of $d(\boldsymbol{\rho})$ is small as well. Therefore, we only calculate the rotational average $d(\rho) = \langle d(\boldsymbol{\rho})\rangle$.

The DMC results for the density profile for several cluster sizes N, up to $N = 40$, are shown in Fig. 4. The panels correspond to four interaction models: smooth/0, smooth/ML, AnIso/0, and AnIso/ML. The Iso models give results similar to the smooth model, and are therefore left out from the figure. For the sake of a clear presentation, we do not show the error bars which can be inferred from the fluctuations of $d(\rho)$ visible especially for small ρ. With increasing N, the small ρ value $d(\rho \to 0)$ converges to the two-dimensional equilibrium density, i.e., the equilibrium coverage. As expected, $d(\rho)$ is more spread out when the He-He interaction is weakened due to the ML interaction, resulting in more diffuse clusters with a smaller central density at $\rho = 0$. The effect from the graphene-He interaction model is smaller but still noticeable: stronger corrugation leads to increased localization and, in the $N \to \infty$ limit, to a higher equilibrium coverage.

Also shown in Fig. 4 are PIMC results for $N = 20$, which agree well with the DMC results (showing that thermal broadening is negligible). The differences are largest for the AnIso/0 model, which proved to be a challenging case for PIMC. There, PIMC predicts an even slightly smaller cluster. The reason is that, according to the PIMC results, the ^{4}He$_{20}$ cluster appears to be close to solidification. Since there is no trial wave function bias towards either the liquid or the solid phase, the PIMC simulation has to find the equilibrium configuration without guidance of the trial wave function. We find that a simulation starting from a solidlike $\sqrt{3} \times \sqrt{3}$ configuration stays solidlike for a very long simulation time before the solid configuration eventually melts. The energy difference between liquid and solid configurations is small for $N = 20$, and therefore an even smaller time step is needed ($\Delta\tau = 1/160$ K) than in the cases of other cluster sizes or other

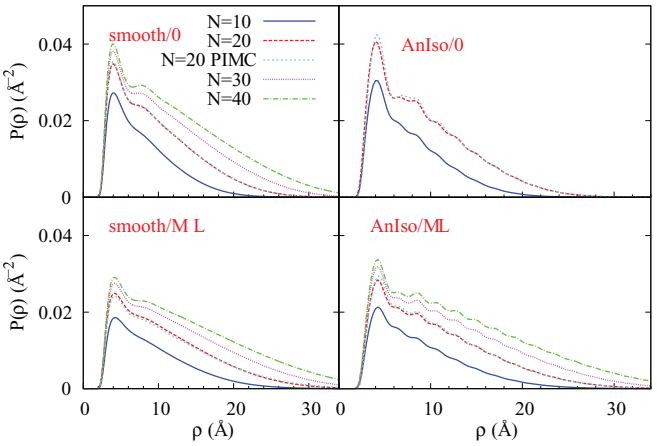

FIG. 5. (Color online) The pair distribution functions $P(\rho)$ as a function of lateral distance for $^4\mathrm{He}_N$ clusters adsorbed on a graphene sheet. The results are obtained by the DMC simulations and, in addition, for $N = 20$, by PIMC. Four He-graphene interaction models are compared in the panels (see also caption of Fig. 4).

interaction models, in order to reduce the bias and ensure the melting of the solid configuration.

It is possible to fit the obtained density profiles to the generalized Fermi profile, using the form given in Ref. 27. Our central densities, obtained from the fit of the DMC distributions for the largest cluster considered are 0.0452(2) Å^{-2} (smooth/0), 0.0458(5) Å^{-2} (Iso/0), 0.0369(2) Å^{-2} (smooth/ML), 0.0396(2) Å^{-2} (AnIso/ML). We can compare our results for the central density to the equilibrium density of liquid ^{4}He on graphene, which was calculated by Gordillo and Boronat who used the isotropic potential.[9] They obtained 0.044 Å^{-2}, which is in good agreement with the values of our central densities, considering that our largest cluster had only 40 atoms.

We also calculate the radial pair distribution function $P(\rho)$ as a probability distribution of particles to be separated in the lateral direction by ρ, which is normalized to the number of particles N. Figure 5 shows $P(\rho)$ for several clusters ($N = 10,20,30,40$) and the four interaction models smooth/0, smooth/ML, AnIso/0, and AnIso/ML. For small ρ, $P(\rho)$ vanishes because of the short-range repulsion of two atoms (the "correlation hole"). As ρ increases, a large peak appears which is the correlation peak always found in pair correlation functions of liquids, classical or quantum. The small modulation of $P(\rho)$ in the case of the AnIso models, beyond the correlation peak, can be explained by the corrugation of the graphene-He potential. If every potential minimum would lead to a higher probability density for ^{4}He, $P(\rho)$ would have maxima for all ρ that equal the distances between these potential minima. However, the repulsion prevents ^{4}He atoms to occupy all minima, so it is rather the $\sqrt{3} \times \sqrt{3}$ lattice sites, corresponding to every third minimum, that have an increased probability in $P(\rho)$. Indeed, we confirm that the small peaks of $P(\rho)$ can be identified as the distances between the sites of the $\sqrt{3} \times \sqrt{3}$ lattice (but note that all results shown in Fig. 5 are for *liquid* clusters). The modulation is less pronounced for the less binding AnIso/ML model, where the clusters are more spread out than for the AnIso/0 model. For the smooth graphene model, of course no such modulation is observed, and $P(\rho)$ is almost featureless beyond the correlation peak.

V. ^{4}He LIQUIDLIKE CLUSTERS ON BOTH SIDES

Suspended graphene sheets allow adsorption on both sides. Hence, it is possible that composite clusters consisting of $^4\mathrm{He}_N$ atoms on one side of graphene and $^4\mathrm{He}_M$ atoms on the other side are formed, as a consequence of the interaction between ^{4}He atoms on opposite sides. We label such clusters by $^4\mathrm{He}_{N,M}$. Note that two ^{4}He atoms on opposite sides are separated by about 5–6 Å . Therefore, they will explore only each other's attractive tail because the repulsion is too short ranged to be felt across a graphene sheet. As long as the graphene-mediated interaction (such as the ML interaction, but also other contributions that we neglect here) does not overcompensate the attraction, it is reasonable to assume that a bound dimer state of $^4\mathrm{He}_{1,1}$ exists. A rigorous proof for the existence of a bound dimer state applies only to attractive particles in strictly two dimensions.[47] Adsorbed ^{4}He atoms are strongly confined in the direction perpendicular to the graphene sheet, but are not strictly two dimensional. Furthermore, in the parallel direction the ^{4}He atoms move in the corrugation potential. Therefore, the existence of a bound dimer state cannot be proven rigorously. Even if it exists, the weak attraction leads to an exponentially small binding energy, which may not be experimentally detectable.

We label the cluster energy of a composite $^4\mathrm{He}_{N,M}$ cluster as $E_{N,M}$. The energy $E_{N,0}$ is then equivalent to the energy E_N from the previous section. We define the additional binding energy $A_{N,M}$ as the energy difference between a composite cluster and two isolated clusters of size N and M: $A_{N,M} \equiv E_{N,M} - (E_N + E_M)$. Figure 6 shows the additional binding energy $A_{N,1}$ of a single ^{4}He atom to a $^4\mathrm{He}_N$ cluster on the opposite side for four different interaction models (smooth/0, smooth/ML, AnIso/0, and AnIso/ML), obtained with the DMC calculations.

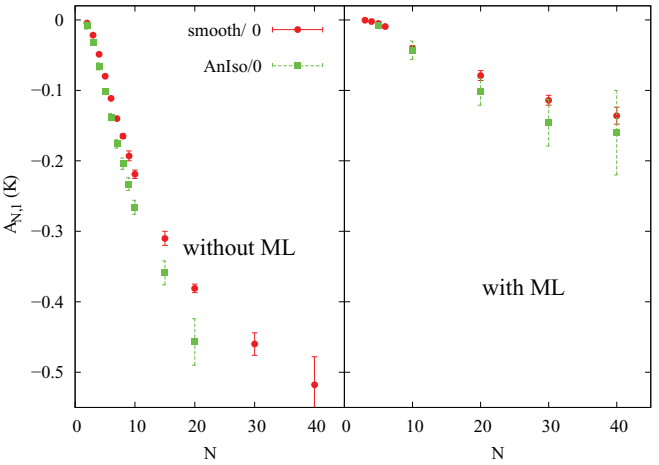

FIG. 6. (Color online) Additional cluster binding energy $A_{N,1}$ of a single ^{4}He atom and a $^4\mathrm{He}_N$ cluster adsorbed on the opposite side of the graphene sheet, as a function of N. The results are obtained using the DMC method and four interaction models (smooth/0, smooth/ML, AnIso/0, and AnIso/ML).

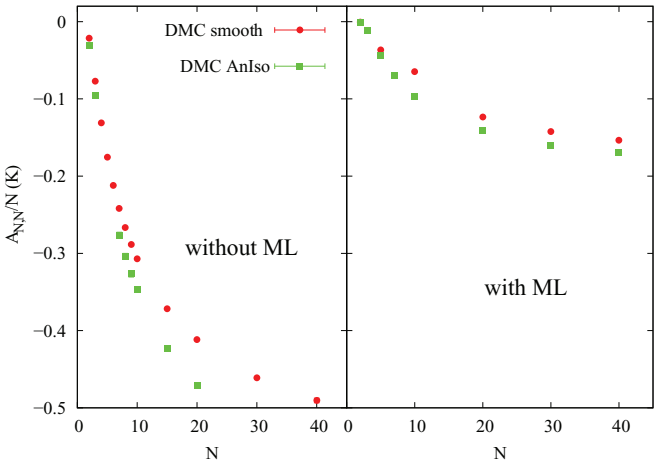

FIG. 7. (Color online) Additional cluster binding energy per particle $A_{N,N}/N$ due to interaction of two $^4\mathrm{He}_N$ clusters adsorbed on opposite sides of the graphene sheet, as a function of N. The results are obtained using the DMC method and four interaction models (smooth/0, smooth/ML, AnIso/0, and AnIso/ML).

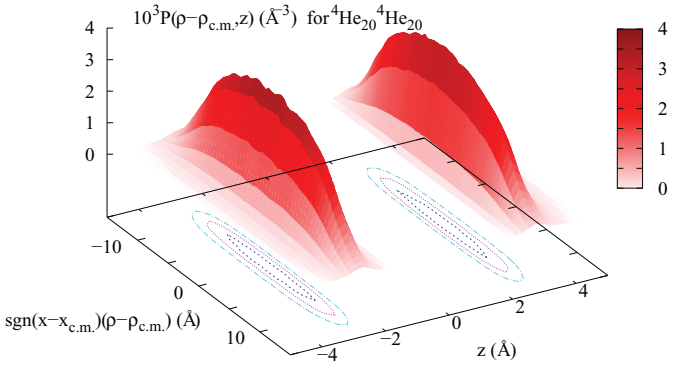

FIG. 8. (Color online) The distribution $P(|\boldsymbol{\rho} - \boldsymbol{\rho}_{\mathrm{c.m.}}|, z)$ of the particles distances to the joint center of mass in the lateral direction and perpendicularly to the graphene plane for $^4\mathrm{He}_{20,20}$ cluster and the AnIso/0 model. The results are obtained using the DMC method. The distance to the center of mass is multiplied by "sgn$(x - x_{\mathrm{c.m.}})$" in order to make visualization more realistic, that is to distinguish the cluster's "left" from "right" side.

As in Sec. IV, we can observe that the ML interaction has a much larger influence on the cluster energy than the corrugation model. When included, the ML interaction significantly reduces $|A_{N,1}|$. With the increase in the number of particles, $A_{N,1}$ decreases, i.e., the binding of a ^{4}He atom to the cluster on the opposite side becomes stronger. It should converge to an asymptotic value $A_{\infty,1}$ which can be estimated perturbatively as the potential energy between an infinite plane of ^{4}He atoms located at $z_0 = -2.8$ Å and a single ^{4}He atom at $z = 2.8$ Å. For a rough estimate, we simply integrate the Lennard-Jones attractive tail over a 2D plane, which results in a potential $V = -2\pi\epsilon\rho\sigma^2(\frac{\sigma}{z-z_0})^4$, with $\sigma = 2.56$ Å and $\epsilon = 10.22$ K. We estimate the area density ρ of a complete ^{4}He layer from the central density given in the previous section. For example, for the smooth/0 model, $\rho \approx 0.045$ Å^{-2}, which yields $A_{\infty,1} \approx -0.8$ K. This is still lower than the value shown in Fig. 6 for $N = 40$ of about -0.5 K, which indicates a slow convergence of $A_{N,1}$ towards $A_{\infty,1}$.

The additional cluster energy per particle for two clusters of the same size, $A_{N,N}/N$, is shown in Fig. 7. Dividing $A_{N,N}$ by N permits the comparison with $A_{N,1}$ given in Fig. 6, in the sense that we are left with N pair interactions contributing to the additional energy in both cases. For small N, $A_{N,1}$ decreases more slowly than $A_{N,N}/N$ because in total there are fewer particles interacting, but for larger N both quantities seem to approach each other and follow the same curve. This can be understood as a consequence of the fact that each cluster is effectively two dimensional and thus, for large clusters, each atom approximately experiences the additional interaction of $A_{N,1}$. Since for large N only a small fraction of particles on the other side are within interaction range, we get $A_{N,N} \approx NA_{N,1}$ for large N.

The spread of clusters on the surface of graphene is probed by a distribution function $P(|\boldsymbol{\rho} - \boldsymbol{\rho}_{\mathrm{c.m.}}|, z)$ which shows the probability density of particles with respect to the distance to the common center of mass in the lateral direction $|\boldsymbol{\rho} - \boldsymbol{\rho}_{\mathrm{c.m.}}|$ and the distance perpendicularly to the graphene plane z. Figure 8 shows $P(|\boldsymbol{\rho} - \boldsymbol{\rho}_{\mathrm{c.m.}}|, z)$ for the $^4\mathrm{He}_{20,20}$ cluster and the AnIso/0 interaction model, obtained using the DMC method. It can be noticed that the two clusters are effectively two dimensional, due to the strong binding to graphene. One can also observe that the respective centers of mass of the two clusters are almost completely aligned in the lateral direction. Similar profiles are obtained when the ML interaction is included, the only difference being the larger spread in the direction of the graphene plane and the lower value of the central density.

In Sec. IV, we have shown the pair distribution function $P(\rho)$ for ^{4}He clusters adsorbed on one side of graphene (Fig. 5). For composite clusters $^4\mathrm{He}_{N,N}$ occupying both sides of graphene, the results for $P(\rho)$ between atoms on the *same* side are almost identical to those in the previous section, and will not be shown. However, the fact that composite clusters are bound, despite the separation by the graphene sheet, raises the question about the strength of pair correlations between atoms on *opposite* sides. In Fig. 9, we show the corresponding pair distribution function $P_o(\rho)$ as a function of the lateral distance, obtained by the DMC method for several N. We again compare the DMC results with the PIMC results for $N = 20$ and find good agreement for the smooth/0, smooth/ML, and AnIso/ML interaction models (the PIMC simulation for the AnIso/0 model is discussed in the following paragraph). The "correlation hole" is missing since the short-range He-He repulsion does not play a role for $P_o(\rho)$: even for $\rho = 0$, the three-dimensional distance is 5–6 Å for ^{4}He atoms on opposite sides, i.e., much larger than the short-range repulsion of the He-He potential. For the AnIso/0 and AnIso/ML model, $P_o(\rho)$ is modulated, similarly to $P(\rho)$. Again, the modulations are simply caused by the minima of the graphene-He interaction. Compared to the modulations of $P(\rho)$, $P_o(\rho)$ has additional peaks which arise because ^{4}He atoms on opposite sides can have higher probability density in potential minima arranged according to the same or two displaced $\sqrt{3} \times \sqrt{3}$ lattices. In order to see more clearly the pure He-He correlations across the graphene sheet, apart from modulations caused by the corrugation, we also calculate $P_o(\rho)$ for the smooth/0 and smooth/ML models, which eliminates the substrate-induced

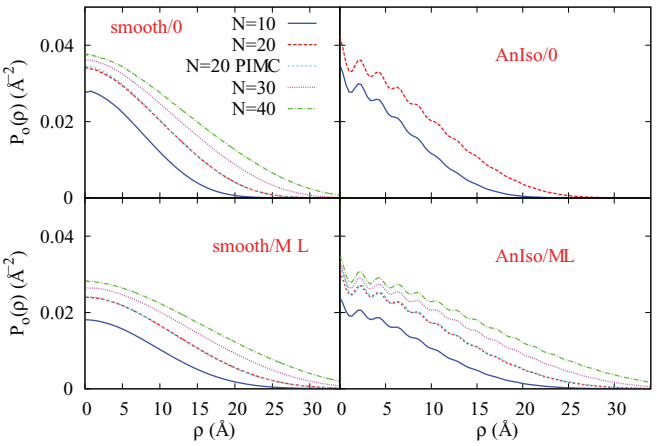

FIG. 9. (Color online) Pair distribution function between atoms on opposite sides of a graphene sheet $P_o(\rho)$ as a function of lateral distance for $^4He_{N,N}$ clusters. The results are obtained by the DMC simulations and in addition, for $N = 20$, by PIMC. Four He-graphene interaction models are compared in the panels (see also caption of Fig. 4).

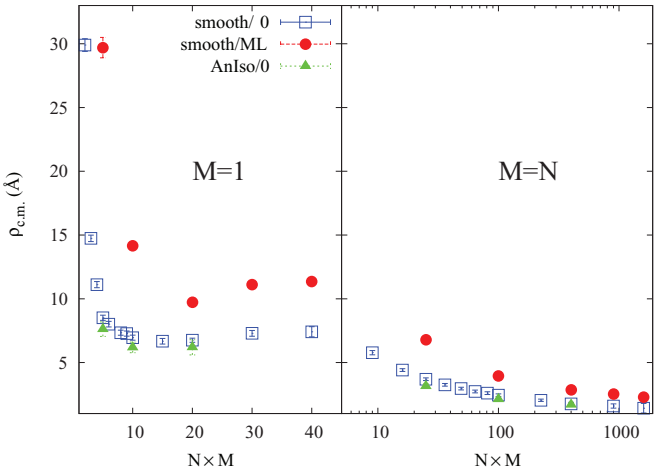

FIG. 10. (Color online) The average lateral separation $\rho_{c.m.}$ of the centers of mass of the upper and lower parts of $^4He_{N,M}$ clusters for $M = 1$ (left) and $M = N$ (right). The results are obtained using the DMC method for the smooth/0, smooth/ML, and AnIso/0 graphene-He interaction models. $\rho_{c.m.}$ is plotted as function of the number of possible pair interaction across the graphene sheet, $N \times M$.

modulations. In this case, $P_o(\rho)$ is completely featureless, exhibiting no discernible peaks. Hence, the pair correlations across the graphene sheet are negligibly weak, at least in the present case of the He-He interaction.

In Fig. 9, we have not presented the PIMC results for the AnIso/0 model in the case of $^4He_{20,20}$ cluster because PIMC does not reach the same equilibrium phase for different initial conditions, despite very long simulation time. If we start the simulation from the solid configuration, the cluster remains solidlike, and if we start from the liquid configuration, the cluster remains liquidlike. The DMC results show that a liquidlike phase is energetically slightly preferred, but the difference in the ground-state energies of the liquidlike and solidlike phases is within the error bars of the PIMC simulations, making it extremely difficult for PIMC to find the energetically more favorable state within reasonable computation time.

We also study the cluster size dependence of the average lateral separation $\rho_{c.m.}$ of the centers of mass of the upper and lower parts of $^4He_{N,M}$ clusters: $\rho_{c.m.} = |\vec{\rho}_{c.m.N} - \vec{\rho}_{c.m.M}|$, where $\vec{\rho}_{c.m.N}$ is the center of mass of the cluster on the upper side of the graphene sheet in the graphene plane, and $\vec{\rho}_{c.m.M}$ is the same quantity for the lower cluster. For small clusters, a convenient parameter to characterize the interactions across the graphene sheet separating the clusters is the number of possible pair interactions $N \times M$ between the N atoms adsorbed on one side and the M atoms adsorbed on the opposite side. Figure 10 shows the dependence of the average separation $\rho_{c.m.}$ on the number of pairs $N \times M$ for $M = 1$ and $M = N$ in the case of three different interaction models.

In the $M = 1$ case, $\rho_{c.m.}$ first decreases steeply with increasing N. This is caused by the stronger binding of the single ^{4}He atom when there are more ^{4}He atoms on the other side of the graphene sheet. $\rho_{c.m.}$ levels off at around $N = 20$, where it attains the minimum separation min[$\rho_{c.m.}$], before rising again for larger N. $\rho_{c.m.}$ is bound to eventually rise with N because as more atoms are added to the cluster of N atoms, they are outside of the interaction range with the single ^{4}He atom on the opposite side. Therefore, the cumulative attraction of a large cluster leads to an essentially flat potential well for the single ^{4}He atom, in which it can move almost freely in lateral direction. For large N, $\rho_{c.m.}$ will be of similar magnitude as the radius of ^4He_N cluster, hence $\rho_{c.m.} \sim \sqrt{N}$. In the limit $N \to \infty$, i.e., full coverage of one side of graphene, the ^{4}He atom on the opposite side will not feel any confining effect of the ^{4}He layer and can move freely in the parallel direction, hence $\rho_{c.m.} \to \infty$. Regarding the model dependence, as expected, min[$\rho_{c.m.}$] is smallest in the AnIso/0 model and equal to 6.1(2) Å, while the smooth/0 model predicts a slightly larger value 6.7(2) Å. The inclusion of the ML interaction, which weakens the He-He attraction across graphene considerably (see Fig. 1), results in an increase of min[$\rho_{c.m.}$]. In the case of the smooth/ML model min[$\rho_{c.m.}$] is 9.7(2) Å.

Unlike in the case of a single ^{4}He atom on one side, for $M = N$ we observe that $\rho_{c.m.}$ decreases monotonically with cluster size. This is understandable from both kinetic and potential energy considerations: (i) the increasing combined mass of N ^{4}He atoms reduces the zero-point motion of their center of mass; and (ii) the cumulative effect of the He-He attraction across the graphene sheet will not lead to a flat central part of the effective potential between the two cluster halves since both halves have equal size. Therefore, it is expected that $\rho_{c.m.} \to 0$ for $N \to \infty$, in case of $M = N$.

The size of a cluster changes when ^{4}He atoms are adsorbed on the other side of a graphene sheet. This effect is very small for large clusters, but can be significant for very small, and thus weakly bound clusters, most notably in the case of a dimer $^4He_2$. Figure 11 shows the DMC results for the average lateral separation $\langle\rho_{12}\rangle$ between the two ^{4}He atoms forming a dimer as a function of the number N of atoms adsorbed on the opposite side of a graphene sheet, for the smooth/0 and smooth/ML interaction models. A similar behavior is expected for corrugated models.

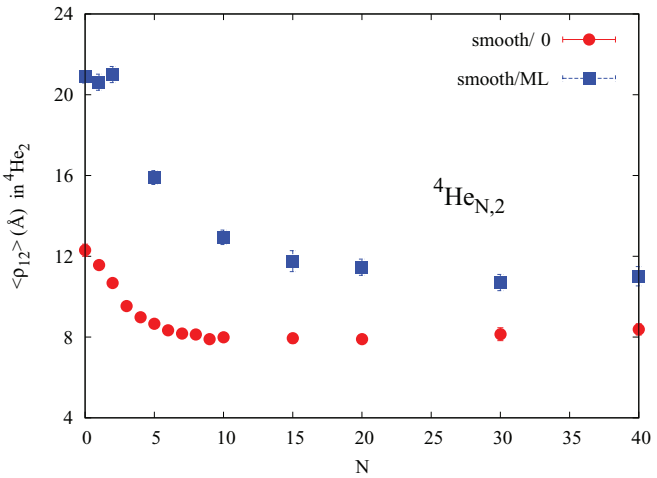

FIG. 11. (Color online) Average lateral separation of the two atoms forming a dimer $^4He_2$ as a function of the number N of ^4He atoms adsorbed on the other side of the graphene sheet. The results are obtained using the DMC method for the smooth/0 and smooth/ML interaction models.

For $N = 0$, helium dimers on graphene have slightly smaller interparticle separations, 12.3(2) Å in smooth/0 model, than in strictly two dimensions, where the average separation between particles is around 13 Å.[48] When atoms are adsorbed on the other side of a graphene sheet they attract the dimer atoms, bringing them closer together. In the case of the smooth/0 model, $\langle\rho_{12}\rangle$ is reduced from 12.3(2) Å for $N = 0$, down to 7.9(4) Å for $N = 9$. When we increase the number of atoms on the opposite side up to $N = 40$, $\langle\rho_{12}\rangle$ remains almost constant within the error bars. For comparison, we note that for $N = 40$ the cluster radius, estimated as a root-mean-square distance to the center of mass is 13–15 Å, depending on the model (see also Fig. 4), i.e., it is already larger than $\langle\rho_{12}\rangle$. If N was increased well beyond $N = 40$, where the size of the cluster opposite to the dimer becomes much larger than typical dimer sizes, $\langle\rho_{12}\rangle$ would increase again since the attraction to the cluster starts to even out laterally and cannot hold the two dimer atoms closer together. For $N \to \infty$, $\langle\rho_{12}\rangle$ should converge to the same value as for $N = 0$, but a study of that convergence would require prohibitively large cluster simulations.

If the ML interaction is included, for $N = 0$ the dimer size increases substantially to 20.8(4) Å. When one atom is added on the other side, the dimer size remains the same within the error bars. The reason is that the resulting interaction is too weak to provide significant additional binding between atoms on opposite sides. Indeed, the additional binding energies $A_{2,1}$ and $A_{1,1}$ are zero within the error bars (although according to the discussion above they are probably bound with an exponentially small binding energy). For $N = 2$, where $A_{2,2}$ is only $-1.1(4)$ mK, the separation of the centers of mass of the two dimers is very large (of the order of 50 Å), and the dimer size remains again the same within the error bars. For $N \geqslant 5$, the additional attraction is sufficient and one observes a reduction of the dimer size as for the smooth/0 model, with an interparticle separation of, e.g., 10.7(4) Å around $N = 30$.

VI. LIQUIDLIKE VERSUS SOLIDLIKE ^{4}He CLUSTERS

In this section, we report the DMC and PIMC results for solidlike clusters for some selected cluster sizes and discuss whether ^4He_N clusters adsorbed on a graphene in its ground state are liquidlike or solidlike. Finite adsorbed ^{4}He clusters allow for a study of solidification in a "bottom-up" approach: while very small clusters are liquidlike for all interaction models we studied, with increase of cluster size a solidlike phase can become favorable, as we found out in the case of the AnIso/0 model. Having in mind that all previous work on ^{4}He adsorbed on graphite and graphene was devoted to the study of bulk phases, i.e., of the thermodynamic limit, studying solidification as a function of cluster size is of fundamental interest.

The DMC simulations have the advantage that, by appropriate choice of the trial wave function, one can study either liquidlike or solidlike phases of the cluster. The comparison of the respective ground-state energies tells us which phase has lower energy and is therefore the true ground state. We label the energies obtained with the liquidlike trial wave function with superscript l, and those with the solidlike trial wave function with s. The AnIso/0 model gives the strongest cluster binding energy in the case of liquidlike clusters and therefore it is the model most likely to predict solidlike clusters beyond a given cluster size.

In the case of $N = 20$, the sites of the optimal solidlike configuration correspond to the expected $\sqrt{3} \times \sqrt{3}$ lattice, arranged such that they form a hexagon of 19 sites with one additional site. For the solidlike cluster energy E^s_{20} we get a range of energies, depending on the strength of the localization to the lattice site, from $-8.23(6)$ K ($\alpha = 0.66$ Å^{-2}), where each ^{4}He atom is well localized, to $-10.5(5)$ K ($\alpha = 0.05$ Å^{-2}), where atoms are no longer confined to a site and the solidlike character has disappeared. The obtained energies are higher than the ground-state energy of the liquidlike cluster $E^l_{20} = -11.40(13)$ K. Thus, we predict that a liquidlike phase is energetically preferred for $^4He_{20}$ in the AnIso/0 model.

However, for $N = 37$ a solid cluster with $\sqrt{3} \times \sqrt{3}$ lattice and the optimal hexagonal shape is clearly preferred: $E^l_{37} = -26.3(2)$ K, $E^s_{37} = -31.27(10)$ K. The choice of lattice sites ρ_I [see Eq. (6)] in the DMC trial wave function is essential. For example for $N = 40$, we compared two clusters with $\sqrt{3} \times \sqrt{3}$ lattice, but with different *shapes*. If the $\sqrt{3} \times \sqrt{3}$ lattices sites are arranged to a hexagon with three additional sites, the solid cluster has a lower energy than the liquid cluster, which is consistent with the result for $N = 37$. However, if the $\sqrt{3} \times \sqrt{3}$ cluster lattice has a rectangular shape (which does not have the minimum "surface" line), the situation reverses: the rectangular-shape cluster with underlying $\sqrt{3} \times \sqrt{3}$ lattice has a higher energy than the liquid cluster of $N = 40$. Hence, we obtain an energy hierarchy solid(hexagonal) < liquid < solid(rectangular). This demonstrates the importance of finite-size effects in that the shape of the cluster is as important as the choice of liquid or solid phase of the trial wave function.

In the case of the AnIso/ML model, we obtained that the liquidlike nature of the ground state is preferable for $N \leqslant 40$, while the energy of the solid configuration is above the liquid, approaching it monotonously when the confinement to the lattice site, controlled by α, is significantly reduced. For the

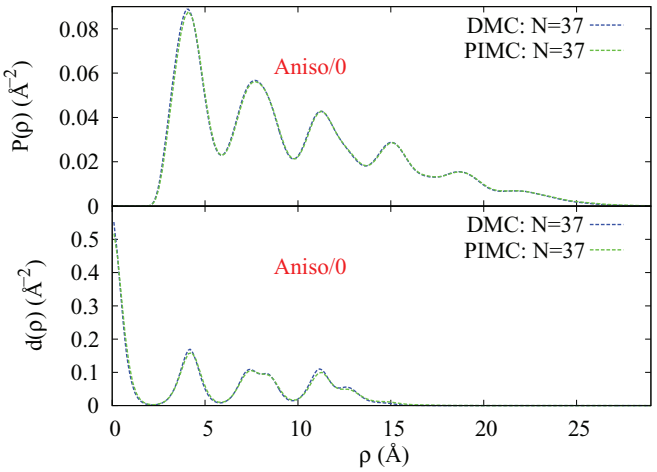

FIG. 12. (Color online) Pair distribution functions $P(\rho)$ (top) and density profiles $d(\rho)$ (bottom) of solidlike cluster $^4He_{37}$ obtained by DMC and PIMC for the AnIso/0 model.

Iso/0 and smooth/0 models, the liquid is still preferred for all studied cluster sizes $N \leqslant 40$, hence also for these models including the ML interaction.

Our DMC results for $N = 37$ are validated by the PIMC results obtained at the temperature of $T = 0.156$ K. The PIMC method does not require a trial wave function, therefore assuming ergodicity PIMC will find the equilibrium state without guidance. On the other hand, the lack of a trial wave function at such low T means that PIMC simulations are not very efficient and ergodicity must not be taken for granted, especially for larger clusters and when the energy differences between liquidlike and solidlike configurations are small. We performed PIMC simulations for both the AnIso/0 and Iso/0 models. In Fig. 12, we compare the pair distribution $P(\rho)$ and density profile $d(\rho)$ obtained with the PIMC to those obtained with the DMC method for $N = 37$. In agreement with the predictions obtained with the DMC method, for the AnIso/0 model our PIMC results predict a solidlike cluster and for the Iso/0 model it predicts a liquidlike cluster. This is illustrated also in Fig. 13, where we show the two-dimensional density $\rho(x,y)$, where (x,y) is defined relative to the center of mass of the cluster. The left and right panels are the result for the Iso/0 and AnIso/0 models, respectively. The $\sqrt{3} \times \sqrt{3}$ lattice structure of the cluster in the AnIso/0 model is very evident, with the same lattice constant as the commensurate

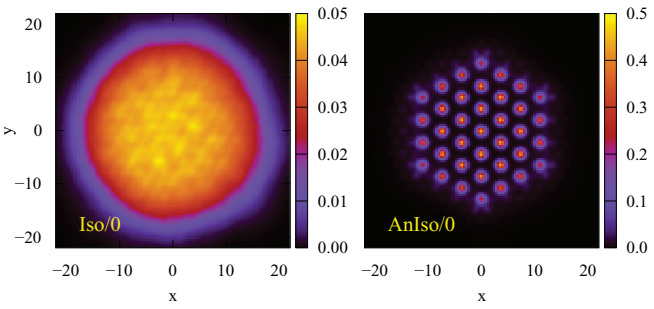

FIG. 13. (Color online) Two-dimensional density $\rho(x,y)$, where (x,y) in Å is defined relative to the center of mass of the cluster. The results are obtained by PIMC method for the $^4He_{37}$ cluster.

lattice, although the height of the density peaks falls off slightly from the center, which indicates that ^{4}He atoms in the center have a smaller zero-point motion than those at the edge of the cluster. Furthermore, the hexagonal shape of the cluster is very well defined, with only a low probability density beyond the hexagonal lattice. This is to be compared with the density $\rho(x,y)$ resulting in the Iso/0 model, shown in the left panel, which is smooth apart from a trivial weak modulation caused by the graphene corrugation.

Our results are consistent with very recent results from Kwon and Ceperley[19] concerning a submonolayer of helium on graphene. In the case of the anisotropic potential model the vacancies did not move, no superfluid fraction was observed, and the peaks in the static structure function indicated that the commensurate $\sqrt{3} \times \sqrt{3}$ phase was preserved, which is consistent with the formation of solidlike clusters separated by localized vacancies. On the other hand, in the case of less corrugated isotropic potential their results indicate a transition from a commensurate solid to a liquid with the decrease of coverage.

VII. CONCLUSIONS

We have studied the ground state of ^4He_N clusters, for $N \leqslant 40$, adsorbed on one and both sides of graphene for six different interaction models for the graphene-He system: adsorption on a smooth graphene surface and, more realistically, on graphene with two different corrugation models; these three models are combined with three-body effects on the He-He interaction due to the substrate-mediated McLachlan interaction. In this way, we were able to estimate the importance of the corrugation and the models used to study it, as well as the influence of the ML interaction which weakens the attraction between He atoms. We find that the ML interaction has a stronger influence on the self-binding properties of the cluster than the model for the corrugation. Omitting the ML interaction more than doubles the cluster energy per particle. While the model for the He-C interaction has less influence on the strength of the cluster self-binding, it is crucial to include corrugation in order to find out if a liquid or solid phase is preferred for a given cluster size. Our results show that for $N = 37$, a solidlike hexagonal-shaped cluster is preferred to a liquidlike cluster only in the AnIso/0 model, where the corrugation is strongest and where the He-He interaction is not weakened by the ML interaction. Thus, for the AnIso/0 model, solidification of ^{4}He clusters adsorbed on a graphene sheet happens somewhere between $N = 20$ and 37. In contrast to that, for all ^4He_N clusters up to $N = 40$, the liquid phase is the energetically preferred ground state when the interaction models AnIso/ML, Iso/0, Iso/ML, smooth/0, and smooth/ML are employed. A systematic search to pinpoint the stability limits of liquidlike versus solidlike clusters in different models and for larger number of particles in the cluster is in progress.

Structural properties of the clusters are also affected by the choice of graphene-He model. The central cluster densities for the largest N of liquidlike clusters, which approach the bulk equilibrium densities, increase from 0.0369(2) Å^{-2} for the least binding smooth/ML model to 0.0458(5) Å^{-2} for the strongest binding model that remains liquid in the studied range, the Iso/0 model. The corrugated models in addition

exhibit small modulations in the pair correlation functions, where peaks beyond the main correlation peak can be related to a slight $\sqrt{3} \times \sqrt{3}$ lattice order in the pair correlations of liquid clusters.

We furthermore studied $^4He_{N,M}$ clusters adsorbed on both sides of graphene and found that two clusters on opposite sides are bound. However, since the He-He attraction across the graphene sheet is very weak, the pair distribution function between the two parts of the composite cluster shows no peaks, i.e., pair correlations between ^{4}He atoms on opposite graphene sides are negligible. Again, the ML interaction has the largest influence on the results, which when included significantly reduces the additional binding. A cluster shrinks in the presence of a cluster on the opposite side, however, this effect is pronounced only for the smallest clusters. The average distance between the atoms of a ^{4}He dimer adsorbed on one side of graphene, depending on the model, is reduced by 35% to 50% as more particles are added on the other side.

In terms of methodology, we have investigated the ^4He_N-graphene system mostly with the DMC simulations, but we also made some finite-temperature PIMC simulations as an independent check for trial-wave-function bias. In the past, both methods have been used successfully for simulations of monolayers of ^{4}He adsorbed on a substrate, which means they are both suitable for monolayer studies. The strength of DMC is the high efficiency of ground-state calculations, provided that a well-optimized trial wave function is used. The strength of PIMC is that a trial wave function is not needed, eliminating a source of bias. In our study of adsorbed ^{4}He clusters, our experience is that DMC is vastly more efficient. Because of the small chemical potential of the clusters, PIMC simulations require a very low temperature to prevent evaporation. For example, large ^{4}He clusters in vacuum have a chemical potential of -7.2 K, and it is known experimentally that they cool to 0.3–0.4 K before evaporation effectively stops. For the small adsorbed ^{4}He clusters studied here, the chemical potential is about an order of magnitude smaller, and we therefore expect evaporation to effectively stop for temperatures below 0.05 K. All our PIMC simulations are actually done at higher T, while monitoring the simulations to make sure that no ^{4}He atoms have evaporated. Even at the temperatures that we use in our PIMC simulations, it is much more expensive to calculate the cluster binding energy compared to DMC. Despite these drawbacks, we got a very good agreement between DMC and PIMC for structural quantities like the radial density profile and the radial pair distribution function. This shows that our choice of trial wave function did not bias the DMC results. PIMC simulations were also helpful in guiding our intuition for larger clusters where PIMC clearly showed that those clusters are solidlike, regardless of the initial configuration of ^{4}He atoms. DMC was then used to answer whether a liquidlike or solidlike state has a lower energy.

ACKNOWLEDGMENTS

The authors would like to thank J. Boronat for helpful discussions. We acknowledge support from the bilateral Projects No. HR-21/2010 and No. HR-26/2012 of the Österreichischer Austauschdienst (OeAD) and the Croatian Ministry of Science, Education and Sports (MSES). L.V.M., P.S., and I.B. acknowledge support from MSES under Grant No. 177-1770508-0493. We also acknowledge the support of the Central Computing Services at the Johannes Kepler University in Linz, where some of the computations were performed. In addition, the resources of the Isabella cluster at Zagreb University Computing Center (Srce) and Croatian National Grid Infrastructure (CRO NGI) were used, as well as the resources of the HYBRID cluster at the University of Split, Faculty of Science.

[1] K. S. Novoselov, A. K. Geim, S. V. Morozov, D. Jiang, Y. Zhang, S. V. Dubonos, I. V. Grigorieva, and A. A. Firsov, Science **306**, 666 (2004).
[2] F. Schedin, A. K. Geim, S. V. Morozov, D. Jiang, E. H. Hill, P. Blake, and K. S. Novoselov, Nat. Mater. **6**, 652 (2007).
[3] A. M. DaSilva and M. W. Cole, J. Low Temp. Phys. **163**, 122 (2011).
[4] Z. Wang, J. Wei, P. Morse, J. G. Dash, O. E. Vilches, and D. H. Cobden, Science **327**, 552 (2010).
[5] Shriram Shivaraman, Robert A. Barton, Xun Yu, Jonathan Alden, Lihong Herman, MVS Chandrashekhar, Jiwoong Park, Paul L. McEuen, Jeevak M. Parpia, Harold G. Craighead, and Michael G. Spencer, Nano Lett. **9**, 3100 (2009).
[6] L. W. Bruch, M. W. Cole, and E. Zaremba, *Physical Adsorption* (Dover, Mineola, NY, 2007).
[7] M. E. Pierce and E. Manousakis, Phys. Rev. Lett. **83**, 5314 (1999).
[8] D. S. Greywall and P. A. Busch, Phys. Rev. Lett. **67**, 3535 (1991).
[9] M. C. Gordillo and J. Boronat, Phys. Rev. Lett. **102**, 085303 (2009).
[10] M. C. Gordillo, C. Cazorla, and J. Boronat, Phys. Rev. B **83**, 121406(R) (2011).
[11] J. M. Gottlieb and L. W. Bruch, Phys. Rev. B **48**, 3943 (1993).
[12] P. A. Whitlock, G. V. Chester, and B. Krishnamachari, Phys. Rev. B **58**, 8704 (1998).
[13] P. A. Whitlock, G. V. Chester, and M. H. Kalos, Phys. Rev. B **38**, 2418 (1988).
[14] B. Krishnamachari and G. V. Chester, Phys. Rev. B **61**, 9677 (2000).
[15] L. W. Bruch, Milton W. Cole, and Hye-Young Kim, J. Phys.: Condens. Matter **22**, 304001 (2010).
[16] M. E. Pierce and E. Manousakis, Phys. Rev. B **62**, 5228 (2000).
[17] W. E. Carlos and M. W. Cole, Surf. Sci. **91**, 339 (1980).
[18] M. W. Cole, D. R. Frankl, and D. L. Goodstein, Rev. Mod. Phys. **53**, 199 (1981).
[19] Y. Kwon and D. M. Ceperley, Phys. Rev. B **85**, 224501 (2012).
[20] M. C. Gordillo and J. Boronat, Phys. Rev. B **85**, 195457 (2012).
[21] M. C. Gordillo and J. Boronat, J. Low Temp. Phys. **171**, 606 (2013).
[22] M. Nava, C. Billman, D. E. Galli, M. W. Cole, and L. Reatto, J. Phys.: Conf. Ser. **400**, 012010 (2012).
[23] M. Nava, D. E. Galli, M. W. Cole, and L. Reatto, Phys. Rev. B **86**, 174509 (2012).
[24] M. Nava, D. E. Galli, M. W. Cole, and L. Reatto, J. Low Temp. Phys. **171**, 699 (2013).

[25]L. Reatto, D. Galli, M. Nava, and M. W. Cole, J. Phys.: Condens. Matter (to be published).
[26]B. Krishnamachari and G. V. Chester, Phys. Rev. B **59**, 8852 (1999).
[27]A. Sarsa, J. Mur-Petit, A. Polls, and J. Navarro, Phys. Rev. B **68**, 224514 (2003).
[28]J. Mur-Petit, A. Sarsa, J. Navarro, and A. Polls, Phys. Rev. B **72**, 104513 (2005).
[29]L. Vranješ and S. Kilić, Phys. Rev. A **65**, 042506 (2002).
[30]S. Kilić and L. Vranješ, Phys. B (Amsterdam) **329–333**, 270 (2003).
[31]Y. Kwon and H. Shin, Phys. Rev. B **82**, 172506 (2010).
[32]H. Shin and Y. Kwon, J. Chem. Phys. **136**, 064514 (2012).
[33]R. A. Aziz, F. R. W. McCourt, and C. C. K. Wong, Mol. Phys. **61**, 1487 (1987).
[34]A. D. McLachlan, Mol. Phys. **7**, 381 (1964).
[35]K. H. Lau and W. Kohn, Surf. Sci. **65**, 607 (1977); K. H. Lau, Solid State Commun. **28**, 757 (1978).
[36]G. Stan and M. W. Cole, Surf. Sci. **395**, 280 (1998).
[37]J. Boronat and J. Casulleras, Phys. Rev. B **49**, 8920 (1994).
[38]J. Casulleras and J. Boronat, Phys. Rev. B **52**, 3654 (1995).
[39]D. M. Ceperley, Rev. Mod. Phys. **67**, 279 (1995).
[40]M. Leino, A. Viel, and R. E. Zillich, J. Chem. Phys. **129**, 184308 (2008).
[41]M. Leino, A. Viel, and R. E. Zillich, J. Chem. Phys. **134**, 024316 (2011).
[42]G. Guillon, A. Zanchet, M. Leino, A. Viel, and R. E. Zillich, J. Phys. Chem. A **115**, 6918 (2011).
[43]P. Stipanović, L. Vranješ Markić, I. Bešlić, and T. Martinić, J. Low Temp. Phys. **166**, 68 (2012).
[44]S. Kilić and L. Vranješ, J. Low Temp. Phys. **134**, 713 (2004).
[45]T. Korona, H. L. Williams, R. Bukowski, B. Jeziorski, and K. Szalewicz, J. Chem. Phys. **106**, 5109 (1997).
[46]S. Kilić, E. Krotscheck, and L. Vranješ, J. Low Temp. Phys. **119**, 715 (2000).
[47]B. Simon, Ann. Phys. (NY) **97**, 279 (1976).
[48]S. Kilić, E. Krotscheck, and R. Zillich, J. Low Temp. Phys. **116**, 245 (1999).